Neural images of pursuit targets in the photoreceptor arrays of male and female houseflies *Musca domestica*

Brian G. Burton* and Simon B. Laughlin[†]

Department of Zoology, University of Cambridge, Downing Street, Cambridge CB2 3EJ, UK

*Present address, Department of Biomedical Engineering, Boston University, 44 Cummington Street, Boston, MA 02215, USA
[†]Author for correspondence (e-mail: s.laughlin@zoo.cam.ac.uk)

Summary

Male houseflies use a sex-specific frontal eye region, the lovespot, to detect and pursue mates. We recorded the electrical responses of photoreceptors to optical stimuli that simulate the signals received by a male or female photoreceptor as a conspecific passes through its field of view. We analysed the ability of male and female frontal photoreceptors to code conspecifics over the range of speeds and distances encountered during pursuit, and reconstructed the neural images of these targets in photoreceptor arrays. A male's lovespot photoreceptor detects a conspecific at twice the distance of a female photoreceptor, largely through better optics. This detection distance greatly exceeds those reported in previous behavioural studies. Lovespot photoreceptors respond more strongly than female photoreceptors to targets tracked during pursuit, with amplitudes reaching 25 mV. The male photoreceptor also has a faster response, exhibits a unique preference for stimuli of 20–30 ms duration that selects for conspecifics and deblurs moving images with response transients. White-noise analysis substantially underestimates these improvements. We conclude that in the lovespot, both optics and phototransduction are specialised to enhance and deblur the neural images of moving targets, and propose that analogous mechanisms may sharpen the neural image still further as it is transferred to visual interneurones.

Key words: photoreceptor, target, tracking, retina, coding, housefly.

Introduction

Flies pursue moving targets using photoreceptors in their frontal eye region. The application of conventional optical stimuli (flashes and the pseudo-random modulations referred to as white noise) has shown that these frontal photoreceptors form a sharper optical image and have faster responses than photoreceptors in other parts of the male eye or in any part of the female eye. These properties should improve the coding of rapidly moving small targets (Hornstein et al., 2000; Burton et al., 2001).

How great is the improvement? To answer this question we have abandoned conventional stimuli, such as flashes and white noise. The conventional stimuli are powerful and convenient because they define the performance of a cell with standard measures (e.g. impulse response, frequency response, SNR), which can be used to derive responses to more realistic stimuli, such as small moving targets (Juusola and French, 1997). However, neuroethologists have long appreciated the value of testing sensory systems with the stimuli that they have evolved to receive (Camhi, 1985). Sensory systems can be so sensitive to natural patterns that they are not properly characterised using conventional stimuli. For example, white-noise stimuli would tell us little about the mechanisms for echolocation in bats. Even in a simpler peripheral system, Rinberg and Davidowitz (2000) found that the cockroach's cercae respond to white-noise air currents in a way that is inconsistent with their responses to more natural air flow.

Natural stimuli are increasingly used in vision research (Reinagel, 2001; Simoncelli and Olshausen, 2001) because visual mechanisms are adapted to their properties. A 'natural' approach to phototransduction is advisable because neurones in the early stages of both vertebrate (Atick and Redlich, 1992) and invertebrate (van Hateren, 1992; Laughlin, 1981) vision are tuned to the statistics of natural images. The processing of natural scene sequences (the time series of intensity generated as a photoreceptor scans across a natural scene) has been examined directly in fly photoreceptors (van Hateren, 1997) and the results suggest that non-linearities improve coding (van Hateren and Snippe, 2001). This role was not apparent from earlier analyses using conventional stimuli (Laughlin et al., 1987; Juusola et al., 1994).

In addition to scanning across natural scenes, flies track moving targets which generate a different image (Wehrhahn, 1979). Tethered houseflies can pick out a moving spot against a moving background, suggesting the existence of a sensory

gate for moving targets somewhere in the fly's brain (Srinivasan and Bernard, 1977). We applied more natural stimuli of known behavioural relevance, i.e. simulated moving targets, to male and female photoreceptors to see how much selectivity for moving targets emerges during phototransduction.

Although both male and female flies track moving targets (Wehrhahn, 1979; Wehrhahn et al., 1982), these stimuli are especially important for the male who must catch a female in a brief and vigorous aerial chase prior to mating. Several observations, largely of houseflies, indicate that the male eye is particularly adapted for the pursuit task. During pursuit, the male housefly tries to keep the female's image in a sex-specific frontal eye region, the 'lovespot'. This region, of roughly 300 facets, points forwards and upwards so that the female is viewed at high contrast against the sky (Wehrhahn, 1979). Contrast is further improved by peculiarities of lovespot R7 and R8 photoreceptors. Instead of expressing distinct photopigments and feeding into a presumed chromatic pathway, as in the female and other parts of the male eye, lovespot R7 and R8 express the same pigment as R1–6 photoreceptors and, like R1–6, feed into the achromatic (contrast) pathway (Hardie, 1985). The lovespot has larger lenses, smaller inter-receptor angles and narrower point spread functions than other eye regions (Land, 1997; Land and Eckert, 1985). These features provide the lovespot with high spatial resolution. Frontal male photoreceptors have faster responses than other photoreceptors in both the female eye (Hornstein et al., 2000) and other parts of the male eye (Burton et al., 2001), providing better temporal resolution.

We recorded the electrical responses of photoreceptors to pursuit stimuli in both sexes of the housefly *Musca domestica*. Using published measurements of the positions and velocities of flies during the chase and our own physiological measurements of photoreceptor point spread functions, we were able to simulate, using a fixed, spatially uniform light source, the signals received by a photoreceptor as a target moves across its axis. The electrical responses to stimuli in the behavioural range of target distances and speeds define the neural images that one fly 'sees' as it chases another. We compare the neural images in the male's lovespot with those formed in the corresponding frontal region of the female retina to show that male lovespot photoreceptors respond particularly strongly to pursuit stimuli, and to evaluate the optical and neural specialisations responsible. White-noise analysis does not adequately predict these responses, emphasising the value of using biologically appropriate stimuli, even at the level of phototransduction.

Materials and methods
Animals and preparation

Intracellular microelectrode recordings were made from R1–6 photoreceptors in both sexes of the housefly *Musca domestica* L., obtained from a culture maintained in our laboratory. Recordings in males were made from the male lovespot, identified as the dorso-frontal eye region where facet diameter is visibly raised (Hardie, 1985). Recordings in females were located in the equivalent position. Microelectrodes were inserted through a small hole cut from the cornea and sealed with high-vacuum silicon grease. Only cells with a resting potential more negative than –60 mV and a maximum dark-adapted response to a 1 ms flash of light of greater than 50 mV were considered for further study.

Stimuli and recording

White-noise stimuli and pursuit stimuli were delivered by a blue-green light-emitting diode (LED, λ_{max}=505 nm; LEDtronics, Torrance, CA, USA) *via* a fluid-filled light guide, subtending an angle of 30° at the eye. Recordings were made at an effective photon flux greater than 5×10^6 s^{-1}, calculated by extrapolating bump counts made under dark-adapted conditions for each photoreceptor. A PC interfaced with an LED driver and an Axoclamp 2A amplifier (Axon Instruments, Union City, CA, USA) controlled the stimuli and recorded the responses. Sampling was usually at 1250 Hz, but was higher for the briefest pursuit stimuli (see below). To avoid aliasing, responses were low-pass-filtered by a 4-pole Butterworth filter with a cut-off frequency of 500 Hz prior to analogue-to-digital conversion.

For a given photoreceptor the stimulus programme was divided into three sections. The first and last consisted of white-noise stimulation, used to assess the stability of the response, to construct Wiener kernels and to form predictions for signal detection analysis (see below). Pursuit stimuli were presented in the middle section. Finally, the electrode was withdrawn from the cell and the electrode noise was recorded for off-line adjustment of photoreceptor noise estimates.

White-noise stimuli

Five Gaussian white-noise stimuli were presented, each 50 times. Each stimulus was 1024 sample points long and was constructed in the frequency domain to have a cut-off frequency of 400 Hz. White-noise stimuli had the same time-averaged intensity as the adapting light and a contrast standard deviation (S.D.) of 0.25 (S.D. of intensity divided by the mean). Stimulus production was at 1250 Hz.

Pursuit stimuli

Pursuit stimuli were generated by modulating the output of the LED. Although a moving target is a spatio-temporal stimulus, it can be simulated using a uniform source because it is experienced by the single photoreceptor as a signal in time only. Here we derive an expression (Equation 4) for this signal from approximations of a target's shape and the actions of the fly's optics.

For analytical simplicity, we model the target's image before filtering by the fly's optics as a 2-D Gaussian function in angular coordinates. We also consider a dark fly against the sky to have practically maximum contrast. With respect to background light intensity, the relative intensity $X(\boldsymbol{\theta},t)$ of the

target as a function of angular position $\boldsymbol{\theta}$ and time t is then defined as:

$$X(\boldsymbol{\theta},t) = 1 - \exp\left[-\frac{4\ln2}{\Delta\rho_x{}^2} \|\boldsymbol{\theta} - \boldsymbol{\theta}_x(t)\|^2 \right], \qquad (1)$$

where $\Delta\rho_x$ is the width of $X(\boldsymbol{\theta},t)$ at half maximum amplitude (also known as the half-width) and $\boldsymbol{\theta}_x(t)$ is the angular position of the target at time t.

In nature, the target would then be filtered by the point-spread function $L(\boldsymbol{\theta})$ of the eye's optics, which approximates another Gaussian function (Snyder, 1979), thus:

$$L(\boldsymbol{\theta},t) = k\exp\left[-\frac{4\ln2}{\Delta\rho^2} \|\boldsymbol{\theta}\|^2 \right], \qquad (2)$$

where $\Delta\rho$, the angular half-width of $L(\boldsymbol{\theta})$, is the photoreceptor's acceptance angle (see below). k is a normalising constant.

The optical image, $I(\boldsymbol{\theta},t)$, of the target on the retina is then the convolution of the target with $L(\boldsymbol{\theta})$:

$$I(\boldsymbol{\theta},t) = X(\boldsymbol{\theta},t) \otimes L(\boldsymbol{\theta}). \qquad (3)$$

For simplicity, consider a photoreceptor whose optical axis is at the origin [$\boldsymbol{\theta}=(0,0)$]. The target passes directly over the photoreceptor at time $t=0$, with an angular speed of ω. Performing the convolution of Equation 3 and substituting ωt for $\|\boldsymbol{\theta}_x(t)\|$, the relative intensity $C(t)$ received by a photoreceptor as a function of time is:

$$C(t) = 1 - \left(\frac{\Delta\rho_x{}^2}{\Delta\rho_x{}^2 + \Delta\rho^2} \right)\exp\left[-\frac{4\ln2}{\Delta\rho_x{}^2 + \Delta\rho^2}\,\omega^2 t^2 \right]. \qquad (4)$$

Note, for off-axis targets, an extra factor of $\exp[-(4\ln2\phi^2)/(\Delta\rho_x{}^2+\Delta\rho^2)]$ is introduced into the second term of Equation 4, where ϕ is eccentricity.

Equation 4 defines the LED light signal delivered to the photoreceptor to simulate the moving target for different target angular widths $\Delta\rho_x$ and angular speeds ω. By inspection, we see that a given stimulus has a duration (width at half maximum amplitude) τ_c of:

$$\tau_c = \Delta\rho_c/\omega, \qquad (5)$$

where

$$\Delta\rho_c{}^2 = \Delta\rho_x{}^2 + \Delta\rho^2. \qquad (6)$$

$\Delta\rho_c$ is equivalent to the width of the target image after filtering by the fly's optics. Similarly, stimulus contrast, ΔC, is:

$$\Delta C = \frac{\Delta\rho_x{}^2}{\Delta\rho_x{}^2 + \Delta\rho^2}. \qquad (7)$$

For the acceptance angle, $\Delta\rho$, angular sensitivity functions were constructed from the responses of dark-adapted photoreceptors to flashes of light delivered from a point source placed at different positions in the photoreceptors' receptive fields (see Burton et al., 2001). $\Delta\rho$ was measured as the half-width of the angular sensitivity function. Mean values for $\Delta\rho$ were 1.25° for males ($N=13$) and 2.45° for females ($N=18$).

These figures were reduced by 20% to 1.00° and 1.96°, respectively, to take account of changes in acuity that occur upon light adaptation (Hardie, 1979).

The number of sampling points and the sampling rate for generating and recording a given pursuit stimulus were chosen to allow simple measurement of response parameters such as amplitude and width. Sampling frequency was usually 1250 Hz, but for brief stimuli (fast moving targets) this figure was raised to maintain at least 16 samples (often 40) per stimulus duration, τ_c. The order in which chasing stimuli were presented was completely randomised. At least 25 responses were recorded for each stimulus for later averaging.

Analysis and presentation

Target detection

To assess the detectability of the photoreceptor's response to a low contrast target, we form the signal-to-noise ratio, $d'=E[\mathbf{A}]/\sigma$, where $E[\mathbf{A}]$ is the expected response amplitude and σ is the standard deviation of photoreceptor noise, both measured after suppressing the effects of noise with the appropriate linear filter (Papoulis, 1991, pp. 384-386). That is, if h(t) is the filter and H(f) its Fourier transform, then

$$E[\mathbf{A}] = \max\{\mathrm{h}(t) \otimes \bar{v}(t)\} \qquad (8)$$

and

$$\sigma^2 = \int_{-\infty}^{\infty} |H(f)|^2 N(f)df, \qquad (9)$$

where $\bar{v}(t)$ is the average (unfiltered) response and N(f) is the (unfiltered) noise power spectral density. For every target, we choose the filter that maximises d' (Papoulis, 1991):

$$H(f) = \bar{V}^*(f)/N(f), \qquad (10)$$

where $\bar{V}(f)$ is the Fourier transform of $\bar{v}(t)$. H(f) is adjusted in the time domain so that the filter impulse response, h(t), has zero baseline.

In our analysis, $\bar{v}(t)$ was generated by convolving photoreceptor impulse responses with contrast signals of the form of Equation 4. Both photoreceptor impulse responses and noise spectra were calculated from white-noise analysis, as described by Burton et al. (2001). Briefly, the impulse response is equal to the inverse Fourier transform of the photoreceptor transfer function. We obtained the transfer function as the ratio of two spectra, the spectrum of the average response to a white-noise stimulus and the spectrum of the stimulus itself. Noise power was calculated as the power spectrum of the residual responses to the white-noise stimulus (individual responses minus the average response). It was then adjusted by subtracting the electrode noise power spectrum. Both impulse response and noise power measures were averaged across several white-noise stimuli.

Wiener kernels

Higher order predictions of the responses to moving targets were calculated by convolving the target stimuli with both the

photoreceptor's impulse response and its second order Wiener kernel (Marmarelis and Marmarelis, 1978). Second-order Wiener kernels were derived according to the correlation method described by Marmarelis and Marmarelis (1978).

Responses to chasing stimuli

The angular width $\Delta\rho_x$ and angular speed ω of the target at the eye may be manipulated to provide absolute distances and flight speeds. If the absolute distance of the target is s and the true width of an animal (or the half-width of a Gaussian function representing the animal) is b, then:

$$s \approx b/\Delta\rho_x, \qquad (11)$$

for $\Delta\rho_x$ expressed in radians. Similarly, if the flight speed of the target is u, then:

$$u = \omega s, \qquad (12)$$

for ω expressed in rad s^{-1}. When referring to the distance of the target in the text, b is assumed to be 4 mm, a figure corresponding roughly with the half-width of a fly.

Results

The simulation of pursuit stimuli

We model the profile of a target fly as a 2-D Gaussian function of peak contrast, –1, seen against a blank background. We choose a Gaussian largely for analytical simplicity (see materials and methods). However, we note that, like a Gaussian, a fly's body and appendages do not form a solid shape but have a low contrast (fuzzy) margin. We take a fly's half-width to be 4 mm, a compromise between the width of a housefly's head (2.2–2.3 mm) and the length of its body (6.5–7.5 mm). The high peak contrast of our model and the blank background are consistent with the observation that males generally track females against the sky (Wehrhahn, 1979). Because flies are dark objects, seen against the bright sky they are likely to have virtually maximum contrast.

The chasing fly is directed by a few simple target cues: the target's angular position, angular width and angular speed (or equivalents, see Materials and methods; Land and Collett, 1974; Wagner, 1986b; Wehrhahn and Hausen, 1980; Wehrhahn et al., 1982). From the perspective of a single photoreceptor, however, which does not have explicit access to place information, the male's view of the female is described only by her angular width $\Delta\rho_x$ and her angular speed ω (Fig. 1A). These parameters are determined by the female's absolute size, distance and relative flight speed, and the male's turning rate. We define likely combinations of $\Delta\rho_x$ and ω by examining published reports of target distance s, flight speed u and angular speed ω, and by applying two geometric relationships (Fig. 1B; see Materials and methods). First, for small targets, angular width, $\Delta\rho_x$, is inversely proportional to distance s, independent of the target's angular speed ω (Fig. 1B, broken lines). Second, for a given flight speed, u, angular speed ω is inversely proportional to distance s (Fig. 1B, solid lines). We consider

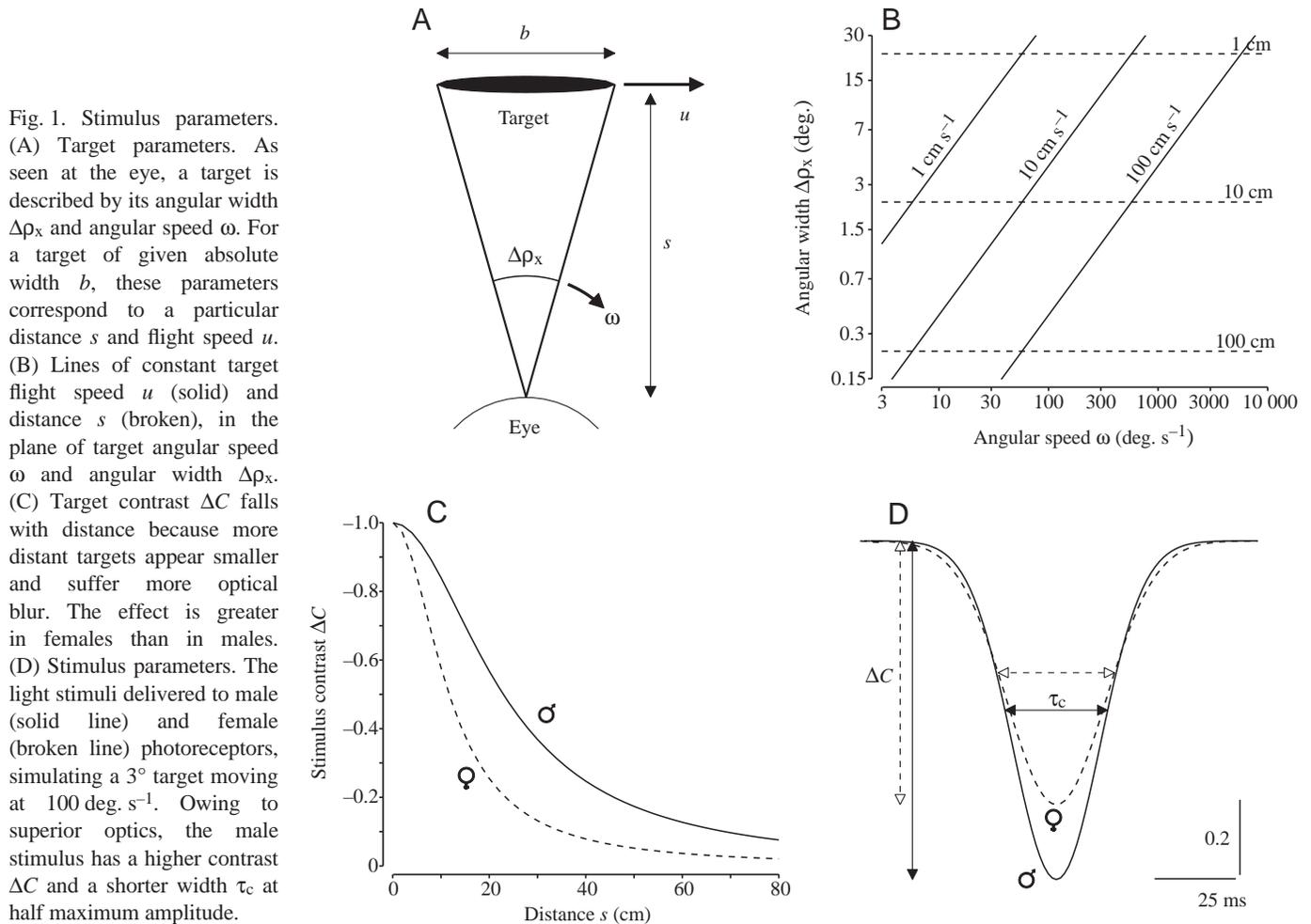two stages of pursuit, the detection of a target and the subsequent chase.

Detection

When a male detects a target, he is either stationary or cruising in a steady forward flight, punctuated by fast 'saccadic' turns >1000 deg. s^{-1} (Schilstra and van Hateren, 1999; Wagner, 1986a). Because saccades occupy a small proportion of the flight, the target's angular speed is usually determined by its flight speed u, relative to the male. *Musca domestica* usually flies at 20–60 cm s^{-1}, but reaches 100 cm s^{-1} in brief bursts (Wagner, 1986a). Thus when a female is detected she is between the 10 cm s^{-1} and 100 cm s^{-1} lines on Fig. 1B. Because the visual space viewed by the lovespot forms a cone, whose volume increases with distance from the animal, a previously unseen target is likely to be distant and will lie below the 10 cm dashed line in Fig. 1B. The optical point spread function reduces the visibility of distant targets by increasing their apparent width and lowering their contrast (Fig. 1C). The male's lovespot has better optics than the female eye. Consequently, target contrast will reach detection threshold at greater distances for males. We set our smallest target width to 0.3°, corresponding to a distance of 76 cm. This distance is well beyond the 20–25 cm at which males orient to other flies (Wagner, 1986b) and is associated with an optical image contrast of less than 10% in both sexes.

Chasing

Chasing is performed at distances of 1–10 cm (Wagner, 1986b), represented in the upper part of Fig. 1B, so we set our largest target width $\Delta\rho_x$ to 30° (a female at <1 cm). At chasing distances the target's optical image has a high contrast (>0.84 in the male's lovespot) and reaches high angular speeds, due to movements by both the target and the chaser. The distribution of angular speeds has not been published but velocity scattergrams show that speeds of 10^2–10^3 deg. s^{-1} are common. Higher speeds occur during the male's saccadic turns (Wagner, 1986b), so we set an upper limit of 10 000 deg. s^{-1}. Our lower limit of 3 deg. s^{-1} is as close as we can practically approach zero in recordings of limited duration.

We simulate a set of targets that cover the behaviourally relevant range of angular widths and speeds as follows. We take a hypothetical target of given angular width and a peak contrast –1.0 against a uniform bright background and blur it with the photoreceptor optical point spread function. A straight track through the centre of this blurred image defines the time-varying contrast signal received by the photoreceptor as the target moves directly across its optical axis (Fig. 1D, see Materials and methods), scaled by angular speed: the faster the target, the shorter the signal duration. This signal is delivered to the photoreceptor by a stationary LED positioned over the optical axis, and the response is recorded. Although the stimulus is spatially uniform, the photoreceptor's response is equivalent to the response to a moving target because photoreceptors show no significant lateral interactions (Smakman and Stavenga, 1987).

Fig. 1. Stimulus parameters. (A) Target parameters. As seen at the eye, a target is described by its angular width $\Delta\rho_x$ and angular speed ω. For a target of given absolute width b, these parameters correspond to a particular distance s and flight speed u. (B) Lines of constant target flight speed u (solid) and distance s (broken), in the plane of target angular speed ω and angular width $\Delta\rho_x$. (C) Target contrast ΔC falls with distance because more distant targets appear smaller and suffer more optical blur. The effect is greater in females than in males. (D) Stimulus parameters. The light stimuli delivered to male (solid line) and female (broken line) photoreceptors, simulating a 3° target moving at 100 deg. s^{-1}. Owing to superior optics, the male stimulus has a higher contrast ΔC and a shorter width τ_c at half maximum amplitude.

Photoreceptor response overview

For the male lovespot photoreceptor (Fig. 2, blue lines), detectable responses first occur around a target size of 0.3° and angular speeds <100 deg. s^{-1} (see below). Response amplitude increases with angular width and the largest responses are in the chasing range (3–30° targets; angular speeds 100–1000 deg. s^{-1}). These chasing responses are biphasic and reach amplitudes (18 mV in this photoreceptor) that are much larger than the response to white noise (Fig. 2, top left trace, above). At higher angular speeds, the responses decrease, the off-transient may remain and the ascending phase can exhibit a notch. Remarkably, the male photoreceptor responds to 3.0° targets (equivalent to a female at 7.6 cm) at the 'saccadic' velocities of 3000 and 10 000 deg. s^{-1}. At the lower speeds, 3–30 deg. s^{-1}, the response amplitude falls slightly, off-transients tend to disappear and the response becomes more symmetrical. When large targets are viewed at the lowest speed the response terminates prematurely, asymmetry increases and off-'transients' reappear. Generally, the most powerful responses run from bottom left to top right in Fig. 2 in the zone commonly occupied by pursuit targets.

The equivalent female responses are smaller and show weaker transients (Fig. 2, red lines), especially for small and fast targets. These sex differences reflect the lower optical contrast experienced by the female photoreceptor (Fig. 1C) and the sexual dimorphism in the frequency response of phototransduction (Hornstein et al., 2000). In the following sections we analyse seven male and seven female photoreceptors to quantify the sex differences in performance under both detection and chasing regimes and to separate the contributions made by optics and phototransduction to response amplitude and duration.

Detection thresholds

The s.d. of voltage noise (corrected for electrode noise) in male and female photoreceptors was 0.205 mV (N=7) and 0.161 mV (N=7) respectively. The photoreceptors' responses to target stimuli approach these values at target widths of around 0.3° for the male and 0.7° for the female. To quantify the response reliability in this 'detection' regime, we performed a conventional 'ideal observer' analysis of the small-target responses of both sexes (Green and Swets, 1966). In this analysis, we imagine a random set of trials in which the fly is presented either with the target or with nothing, with equal probability. On each trial, the photoreceptor response is optimally filtered to amplify the target, if present, and to
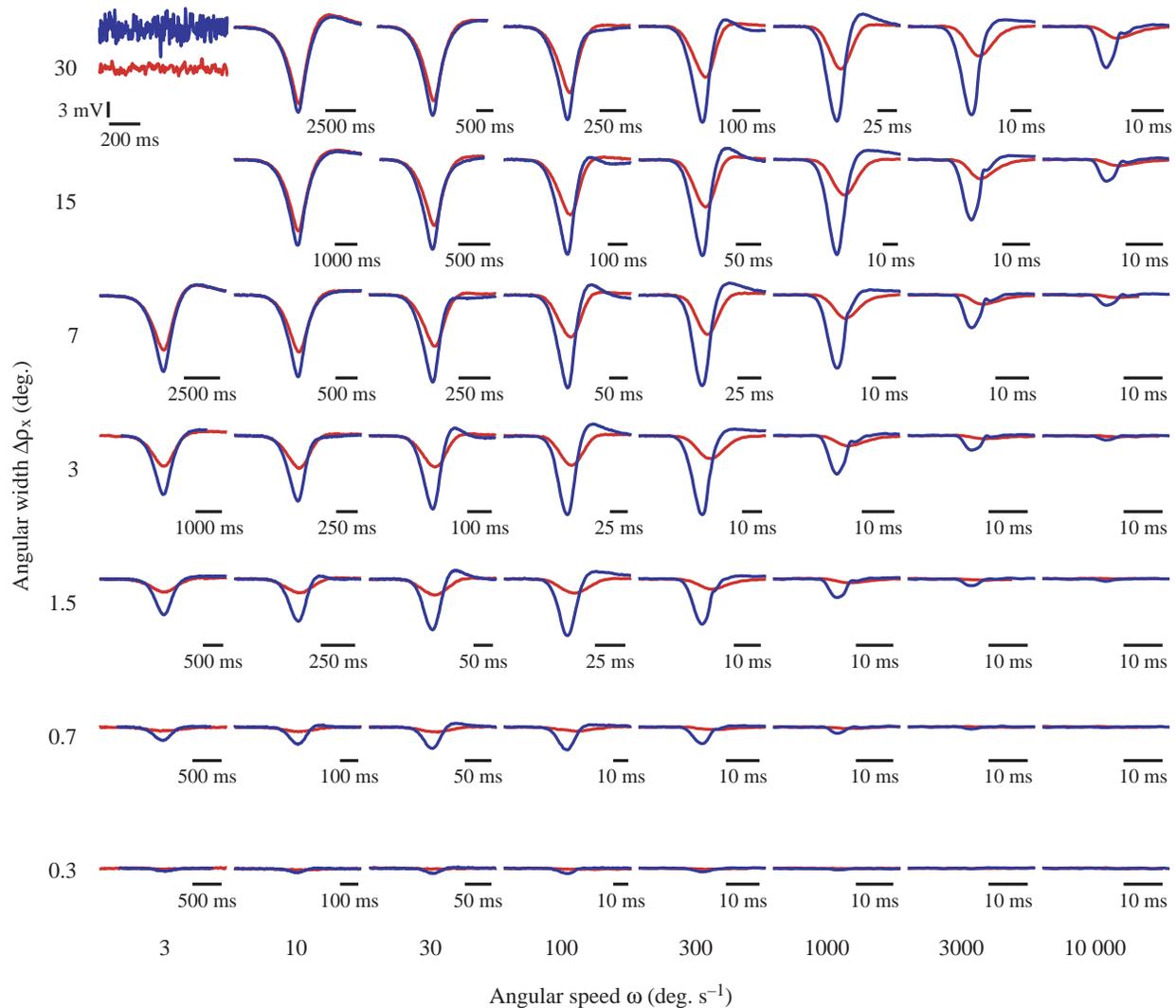
Fig. 2. Male and female pursuit responses. Traces show the mean response (*N*=25) of a male (blue) photoreceptor and a female (red) photoreceptor to a simulated moving target of specified angular width and angular speed. Vertical range is 24 mV. Traces are centred on the peak of the male response and the time axes are scaled by male response duration. The top left plot shows the responses of the same cells to conventional white-noise stimuli (contrast, 25%; cut-off frequency, 400 Hz), male response (blue) above, female response (red) below.

suppress intracellular and photon noise. The observer then decides whether the target was presented on that trial based on the amplitude, **A**, of the filtered response. The performance of an ideal observer at this task is related to a signal-to-noise ratio, $d'=E[\mathbf{A}]/\sigma$, where $E[\mathbf{A}]$ is the expected filtered response amplitude and σ is the S.D. of the filtered noise. The optimal decision rule is to identify the target as present whenever $\mathbf{A}/\sigma>d'/2$. The greater d', the more frequently the observer will be correct.

The expected signal $E[\mathbf{A}]$ may be calculated using mean target responses. However, the means we obtained were still highly corrupted by photoreceptor and electrode noise. Instead, we formed predictions of these responses from impulse responses obtained by white-noise analysis. As we show later, this is a valid procedure in the detection regime as the photoreceptor responds linearly to low-contrast stimuli. σ was

also obtained from white-noise analysis (see Materials and methods). In Fig. 3 we plot d' for all target speeds and for small targets in both sexes. Comparing these values to the 5% error level, we see that the male response to 0.3° targets provides satisfactory amplitudes at target speeds of up to 300 deg. s^{-1}. The female performs nearly as well at the same speeds when the target width is 0.7°. A fly is 0.3° across at a distance of 76 cm. At this distance, an angular speed of 300 deg. s^{-1} corresponds to an absolute speed of 4.0 m s^{-1}, well beyond the normal flight speed of a conspecific. We conclude that, despite choosing stimuli that comfortably include the behavioural range of distances, the male photoreceptor is still providing detectable signals at distances beyond that range.

Response amplitude and contrast amplification

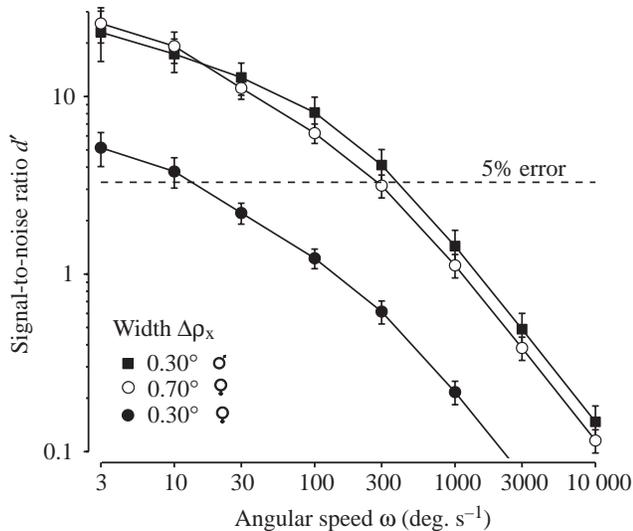Although responses can be biphasic (Fig. 2), for uniformity

Fig. 3. Target detection. Signal detection analysis of predicted target responses at small target widths (large distances) in 7 male and 7 female photoreceptors. The signal-to-noise ratio, d', measures mean response amplitude divided by photoreceptor noise S.D. after filtering responses to suppress noise. Values are means ± S.D. Also plotted is an error line that shows the value of d' (3.29) at which an ideal observer would incorrectly identify signal-present and signal-absent trials 5% of the time in an experiment in which half the trials do not contain a target and when the noise is Gaussian.

with previous studies we define response amplitude ΔV as the maximum hyperpolarisation from the background membrane potential. Following previous studies (Juusola and French, 1997; Srinivasan and Bernard, 1975), we plot ΔV against target angular speed ω (Fig. 4A,B). The male response is larger and, unlike the female, peaks in the chasing range 100–1000 deg. s^{-1}. The peak shifts to higher speeds for larger (nearer) targets.

To place the data in their behavioural context, we replot ΔV against the target speed u in cm s^{-1}, according to the target distance s (Fig. 5A,B). In both sexes the response amplitude falls as the target moves further away and subtends a smaller angle because optical blur reduces contrast (Fig. 1C). At any given target distance and speed, the male response is much larger than the female and the male photoreceptor is adapted to respond to other houseflies by responding most vigorously to targets travelling at normal *Musca* flight speeds of 20–60 cm s^{-1}.

Further analysis separates the contributions made by optics and phototransduction to improving the male response. The lovespot's narrower point spread function increases the peak contrast ΔC and reduces the duration at half peak contrast τ_c of the optical signals produced by moving targets (Fig. 1C,D). We normalise for contrast by taking the ratio, $\Delta V/\Delta C$, and take account of differences in stimulus duration by plotting this ratio against τ_c. With these adjustments, male photoreceptors are still consistently more responsive than female photoreceptors (Fig. 6A,B), indicating that male photoreceptors have a higher gain.

The sex-specific differences in photoreceptor gain can be determined at stimulus durations that are brief enough to generate impulse responses. For $\tau_c <7$ ms, the contrast amplification $\Delta V/\Delta C$ is proportional to stimulus duration (Fig. 6A,B), consequently ΔV is proportional to stimulus energy (the product of duration and contrast). The slope of this relationship (ΔV divided by stimulus energy) defines a gain that is over four times greater in the male photoreceptor (3200±450 mV s^{-1}, $N=7$) than in the female (720±295 mV s^{-1}, $N=7$).

Male photoreceptors maintain a higher gain when stimulus duration increases. For a stimulus of near maximum contrast ($\Delta\rho_x=30°$; $s=0.76$ cm), and near optimum duration ($\tau_c \approx 30$ ms), the male's contrast amplification ($\Delta V/\Delta C=21.6±3.4$ mV, $N=7$), is over three times that of the female ($\Delta V/\Delta C=6.31±2.00$ mV, $N=7$) (Fig. 6A,B). Even at the longest stimulus duration, $\tau_c \approx 3$ s, where the female response is largest (Fig. 6A,B), the male is still more sensitive ($\Delta V/\Delta C=16.2±1.7$ mV, $N=7$; cf.11.4±2.4 mV, $N=7$, in the female). When the stimulus duration τ_c is >7 ms, male photoreceptors amplify high-contrast targets more than low-contrast targets (Fig. 6A), but females only show this non-linearity at the longest stimulus durations, $\tau_c>100$ ms (Fig. 6B). Consequently only male photoreceptors preferentially boost close-quarter pursuit stimuli, which are of short duration and high contrast, above more distant stimuli.

Male photoreceptor gain is highest when the stimulus duration is between 10–30 ms (Fig. 6A). It is this simple time dependency that tunes the male photoreceptor to a female's flight speed, independent of distance (see Fig. 5A). Because the angular speed ω and angular width $\Delta\rho_x$ of a female moving at fixed velocity both fall linearly with viewing distance, a given flight speed always roughly corresponds with a particular stimulus duration (approximately the ratio $\Delta\rho_x/\omega$). Thus, by having cells respond maximally to a particular stimulus duration, a robust preference for the flight speed of a prospective mate is generated without recourse to complicated neural circuitry.

The effects of optical blur and motion blur on spatial localisation

Motion blur, the loss of spatial resolution for moving images, results from the finite duration of the neural response, and combines with optical blur to determine the width of a target's neural image. The angular width of the neural image $\Delta\rho_v$ (in the direction of motion) is the product $\omega\tau_v$, where ω is angular target speed and τ_v is the duration of the photoreceptor voltage response to this moving target at half maximum amplitude. Models of motion blur in insects have made clear predictions (Juusola and French, 1997; Srinivasan and Bernard, 1975). At low image speeds optical blur dominates so that the width of the neural image $\Delta\rho_v$ approximately equals the width of the target after optical blurring $\Delta\rho_c$. At high image speeds, the photoreceptor response duration τ_v is limited by its impulse response, motion blur dominates and the angular width of the neural image $\Delta\rho_v$ increases linearly with target speed.
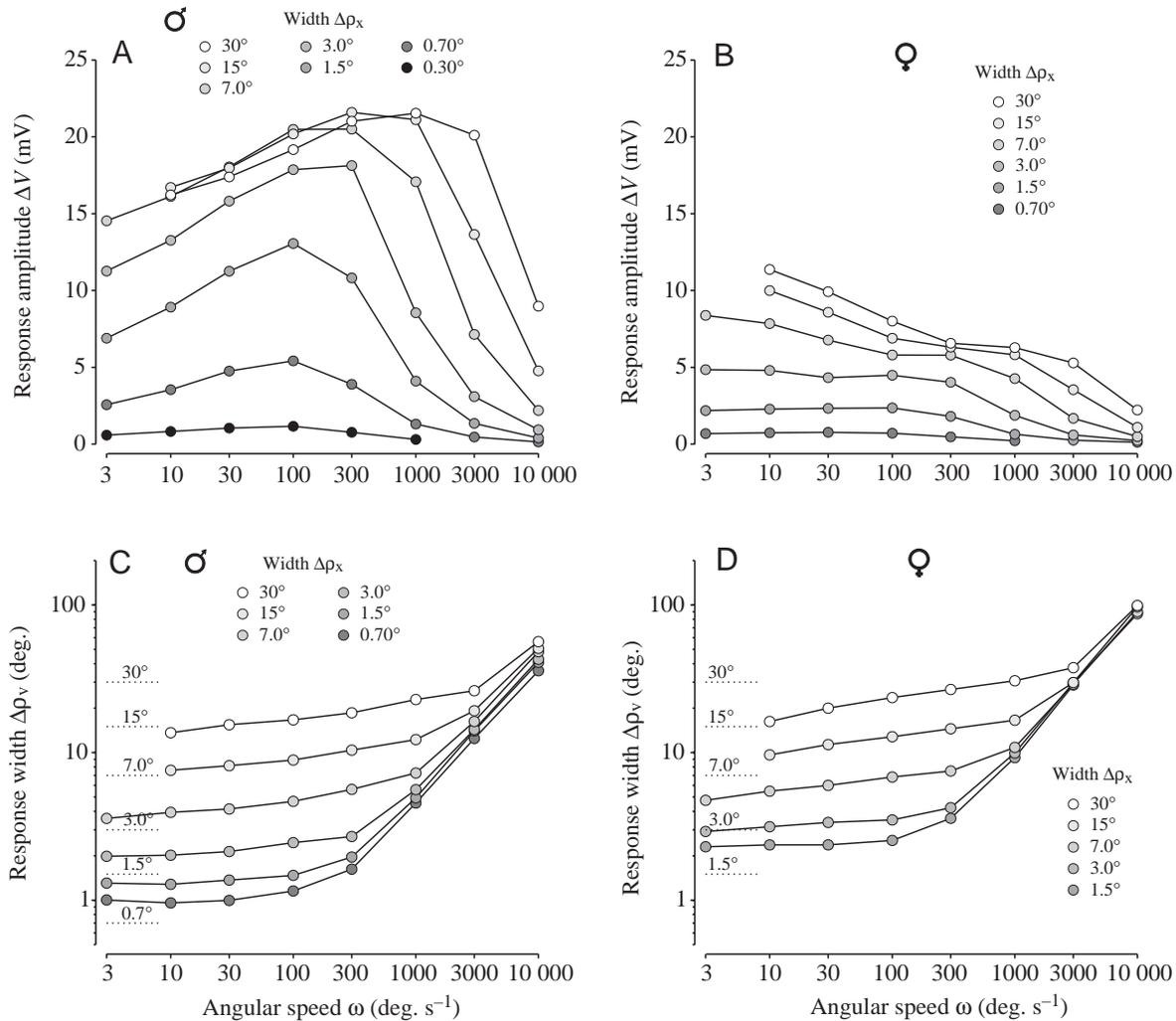
Fig. 4. Effects of angular target speed on response amplitude and image blur. (A,B) Mean response amplitudes ΔV of 7 male (A) and 7 female (B) photoreceptors to simulated target stimuli, plotted against angular target speed ω. The male response is larger than the female response and demonstrates an optimum angular speed that increases with target size. (C,D) Mean angular response width $\Delta\rho_v$ of the same male (C) and female (D) photoreceptors to simulated target stimuli, plotted against angular target speed ω. At low speeds, response widths are less than the widths of the targets (indicated by dotted lines), especially in the male. At high speeds, response width increases with speed (motion blur).

These two regimes are evident (Fig. 4C,D) for both sexes but at low speeds our data depart from previous models. Surprisingly, the neural width drops below the optical width and, in the extreme, is narrower than the target itself (i.e. $\Delta\rho_v < \Delta\rho_x$, as indicated by the broken lines). This sharpening must be neural, as opposed to optical. Some of this neural sharpening can be attributed to the band-pass nature of the photoreceptor response, which produces transients (Fig. 2). However, in a linear system the neural image should asymptote to the optical width $\Delta\rho_c$ when the target speed approaches zero. The fact that it does not in Fig. 4C,D suggests that the photoreceptor is not a simple linear filter. Instead, additional dynamic mechanisms must be operating to shorten responses to longer stimuli and maintain a low blur factor for even very slow moving targets.

Because the neural image of a large target can tolerate more

blur than that of a small target, we define a *blur factor* as the ratio of the angular widths of the neural image and the target, $\Delta\rho_v/\Delta\rho_x$. Plots of blur factor against target speed u (Fig. 5C,D) for the three closest targets (s=0.76, 1.5 and 3.3 cm, equivalent to angular widths of 30°, 15° and 7°) are almost identical, with blur factors <1 up to a speed of $\approx$50 cm s^{-1} in the male, compared with $\approx$15 cm s^{-1} in the female. The precise figures for a 30° (s=0.76 cm) target, derived by linear interpolation of measured points on log–log axes, are 49.5±3.3 cm s^{-1} (N=7) and 14.4±8.1 cm s^{-1} (N=7). Note that for the male the blur factor is <1 over much of the normal range of flight speeds. Males are also more effective at sharpening small targets. For a target width of 1.5° (s=15 cm), the male's blur factor is <1 for speeds up to 27.3±5.4 cm s^{-1} (N=7) (Fig. 5C), but the female's is never <1, and reaches 2 at 40 cm s^{-1} (Fig. 5D).

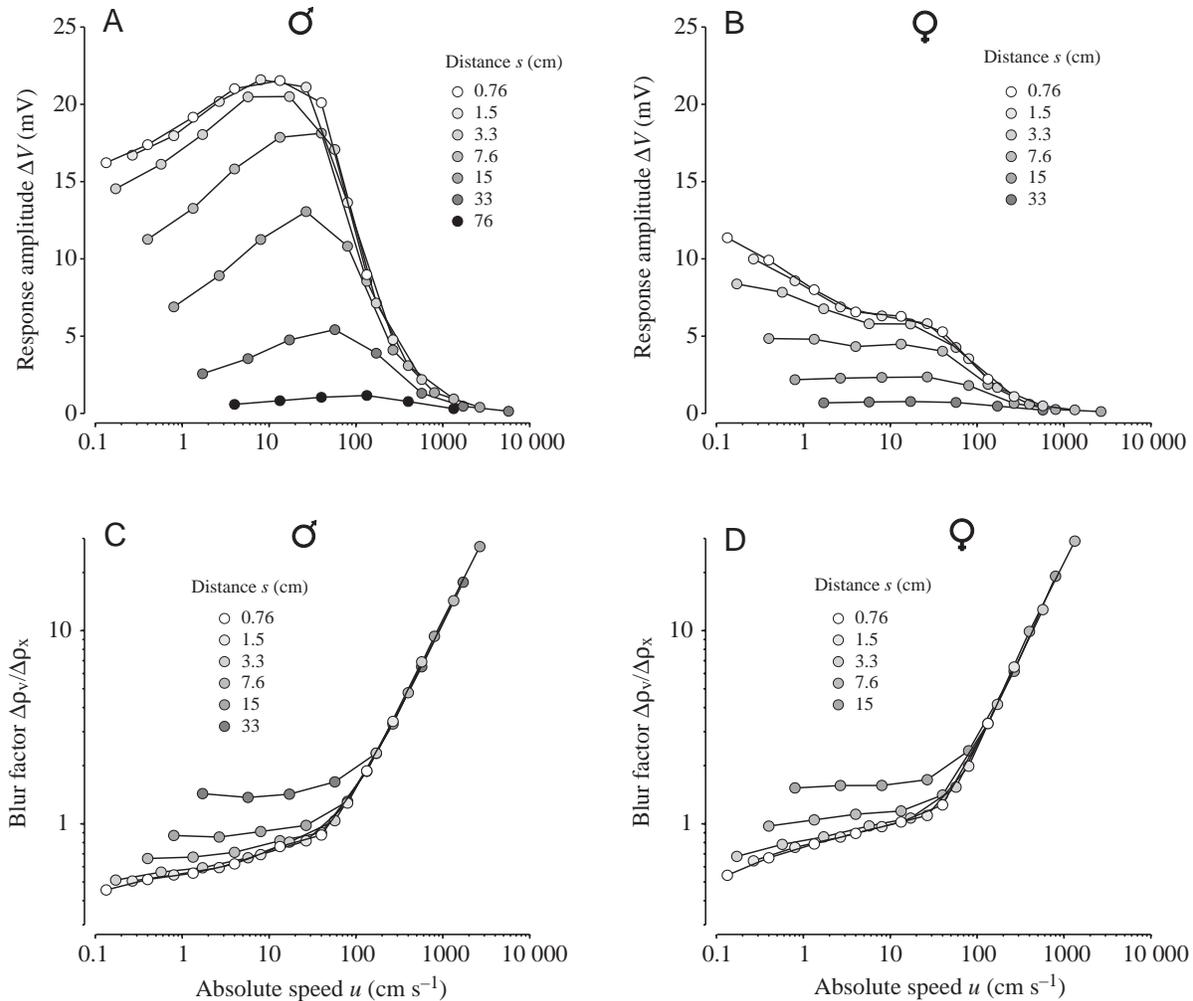The female photoreceptor performs worse than the male

Fig. 5. Effects of absolute target speed on response amplitude and image blur. (A,B) Mean response amplitudes ΔV of 7 male (A) and 7 female (B) photoreceptors to simulated target stimuli, plotted against absolute target speed u. The optimum male response occurs at speeds between 10 cm s^{-1} and 80 cm s^{-1}, for targets at distances of up to 33 cm. (C,D) Mean spatial blur factor $\Delta\rho_v/\Delta\rho_x$ of the same male (C) and female (D) photoreceptors to simulated target stimuli, plotted against absolute target speed u. The male achieves blur factors of less than 1 for slow moving targets at distances of <15 cm. Motion blur begins in both sexes when the target is travelling at approximately 50 cm s^{-1}.

because it has poorer optics and slower and less transient electrical response. We take account of optical differences by defining a second blur factor as the ratio of the durations of photoreceptor response and stimulus waveform, τ_v/τ_c. This factor is plotted against stimulus duration τ_c in Fig. 6C,D. The male clearly shortens the duration of its response more than the female for long duration stimuli, corresponding with slow moving targets. Furthermore, this difference increases for higher contrast stimuli. Therefore, as with response amplitude, blur factor exhibits a non-linear dependency on contrast that is stronger in the male.

In both sexes motion blur dominates at target speeds greater than 50 cm s^{-1} (Fig. 5C,D) where neural image width increases in proportion to both target speed and impulse response duration (Juusola and French, 1997; Srinivasan and Bernard, 1975). Fitting lines to the short duration (fast target) regime of Fig. 6C,D gives impulse response durations (width at half

maximum height) of 4.90±0.33 ms (*N*=7) in males and 9.54±1.79 ms (*N*=7) in females. Although male photoreceptors have faster responses than female photoreceptors, they also suffer less optical blurring. Because motion blur starts to dominate when the impulse response duration exceeds the duration of the optical signal, these factors tend to cancel out. This observation explains why the motion blur regime begins at roughly the same speed, u, in both sexes (Fig. 5C,D).

In summary, the blur factors in males are consistently lower than in females for any target size and speed because the male photoreceptors have better optics and faster, more band-pass responses.

What does the neural image of a moving target look like?

We reconstruct the neural images of targets that males and females 'see' during pursuit from recordings of responses to simulated targets. We incorporate the sex-specific differences
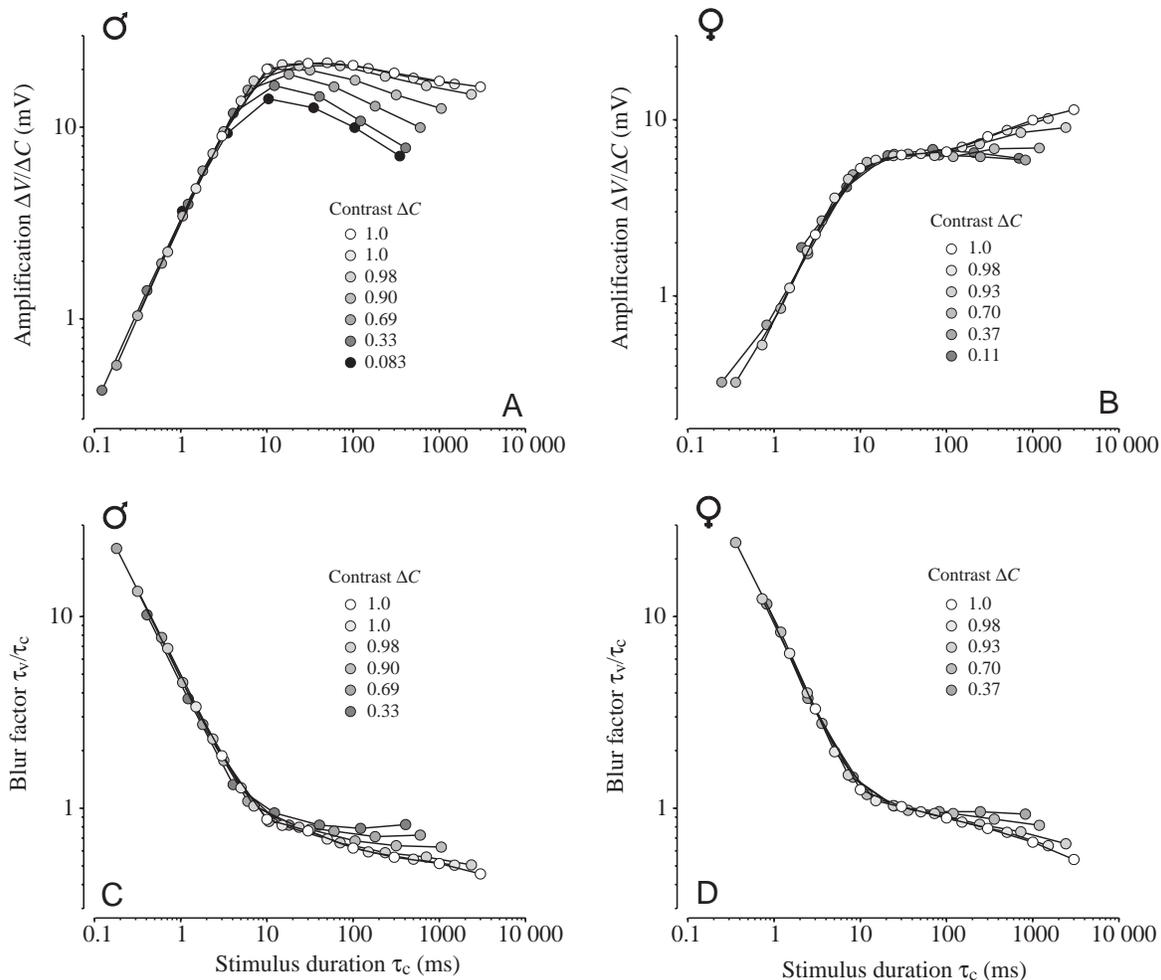
Fig. 6. Effects of stimulus duration on response amplitude and image blur. (A,B) Mean contrast amplification $\Delta V/\Delta C$ of 7 male (A) and 7 female (B) photoreceptors to simulated target stimuli plotted against stimulus duration τ_c. Males preferentially amplify high contrast (near) stimuli. The amplification performed by the female photoreceptor is less powerful than that of the male photoreceptor and exhibits non-linear contrast gain at only the longest durations. Below 4 or 5 ms in both sexes, the response decreases as stimulus power declines. (C,D) Mean temporal blur factor τ_v/τ_c of the same male (C) and female (D) photoreceptors to simulated target stimuli, plotted against stimulus duration τ_c. The male blur factor is always less than the female's for stimuli of comparable contrast, especially at high contrast. Motion blur occurs at stimulus durations below 10 ms.

in photoreceptor sampling densities (Land, 1997; Land and Eckert, 1985), optical point spread functions and electrical responses. With the data recorded so far (responses to targets that pass through the centre of a photoreceptor's field of view) we can only reconstruct the neural image along a single row of photoreceptors, aligned with the target's trajectory. To reconstruct the two-dimensional neural image formed in the photoreceptor array we must measure the responses of photoreceptors in adjacent rows, which view the target obliquely. Accordingly, we simulated the intensity signals received by male and female photoreceptors as targets moved at different eccentricities (see Materials and methods) and applied these stimuli to male and female photoreceptors. For a given target, 22 eccentricities were considered and the responses of photoreceptors were averaged across 30 (male) or 40 (female) presentations. For reasons of space, we present the

reconstructed neural image of just one target, with angular width 3.44° and angular speed 180 deg. s^{-1} (Fig. 7). This is typical of targets encountered during pursuit and gives a stimulus duration of 20 ms, the optimum duration for a male fly (Fig. 6A,C).

Fig. 7 presents different images of the target at a single instant. Contours in Fig. 7A–C show the Gaussian light intensity distributions of the target before (Fig. 7A) and after blurring by male (Fig. 7B) and female (Fig. 7C) optics. Vertical lines indicate the width at half maximum amplitude in each case. The contours in Fig. 7D,E show the photoreceptor voltage responses for males and females, plotted continuously over all retinal positions without regard for the photoreceptor sampling lattice. Fig. 7F,G present these neural images, sampled discretely by the male and female photoreceptor arrays.
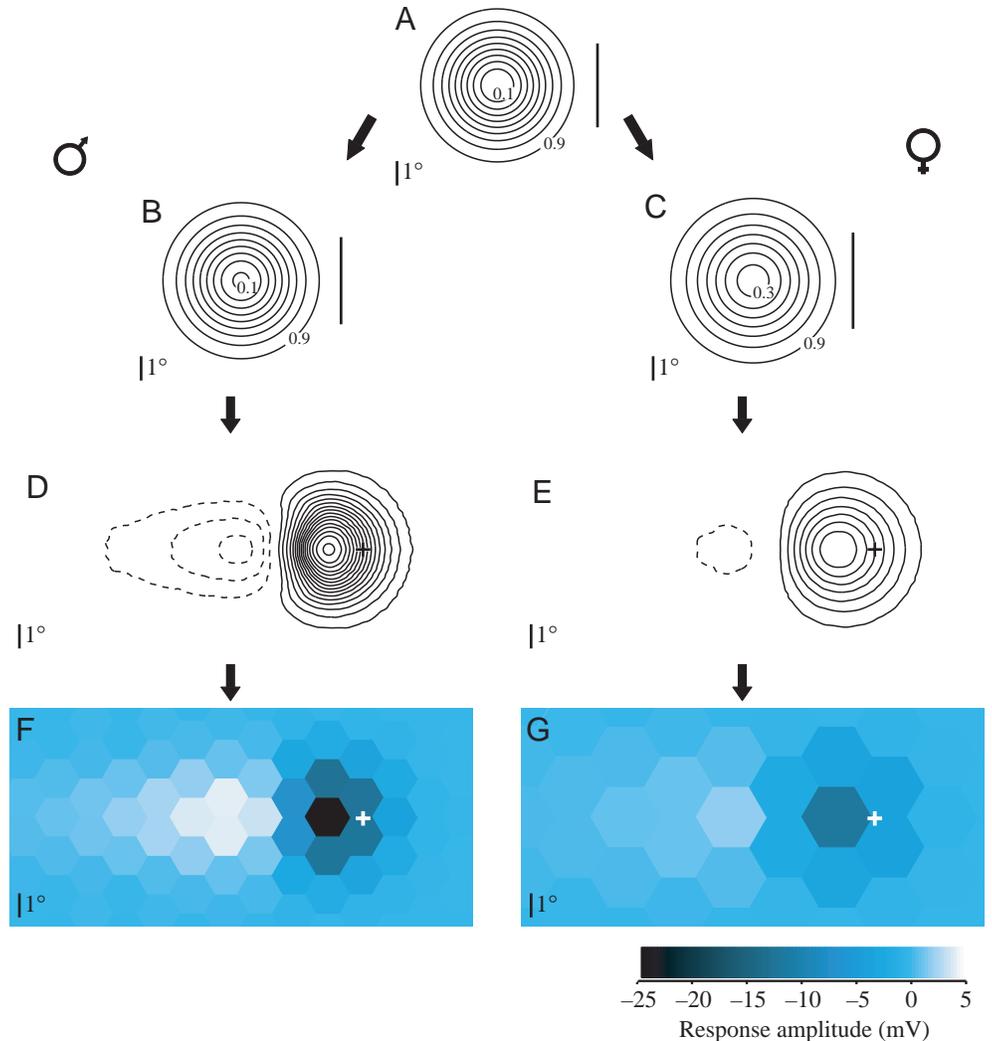
Fig. 7. Neural images of a moving target. (A–C) Contour plots of the angular distribution of relative intensity from a 3.44° target, seen at the eye (A) and after blurring by male (B) and female (C) optics. Contour lines are spaced at intervals of 0.1. The lines on far right indicate half-width. (D,E) Snapshots of the distribution of photoreceptor voltage responses to the same target moving at 180 deg. s^{-1} from left to right as reconstructed for male (D) and female (E) retinas. Crosses indicate the current position of the target. (F,G) Sampled retinal images of the moving target for male (F) and female (G) retinas. Colour patches represent the instantaneous voltage responses of individual photoreceptors separated at angles appropriate for males (1.6°) and females (2.5°).

These reconstructions demonstrate just how much better the male's optics and photoresponses are than the female's at increasing the amplitude of the target's neural image and reducing its width. After optical blurring, the target contrast ΔC is 0.92 in the male but 0.755 in the female, a difference of 22% (Figs 1C, 7B,C). Target width is increased by 4% in the male from $\Delta\rho_x$=3.44° to $\Delta\rho_c$=3.58° (Fig. 7B) but by 15% in the female to $\Delta\rho_c$=3.96° (Fig. 7C). These discrepancies are even larger in the final neural images owing to the larger amplitude of the male's photoreceptor response, its more non-linear contrast gain and more band-pass dynamics. The peak neural response is 24.5 mV in the male and only 11.9 mV in the female, now a difference of 106% (Fig. 7D,E). In the male, the widths of the retinal representation parallel and perpendicular to the direction of motion are 2.77° and 3.23°, respectively. In females these widths are 3.62° and 3.56°. A more rapid, more biphasic male response (compare the depolarising responses behind the target in Fig. 7D,E) also reduces spatial lag. In contour plots (Fig. 7D,E) the peak of the male response lags 1.4° behind the true position of the target, equivalent to a delay of 7.8 ms. In the female the lag is 1.5°,

equivalent to a delay of 8.3 ms. Finally we note that the male's improved spatial resolution is roughly matched by the higher sampling density of his retina (Fig. 7F,G).

Kernels derived from white-noise analysis do not predict pursuit responses

Here we demonstrate the importance of using behaviourally appropriate stimuli by showing that white-noise analysis fails to describe the neural image of near, moving targets. Photoreceptor responses to white-noise stimulation are usually linear (French, 1980; Juusola et al., 1994). Accordingly, Juusola and French (1997) used linear system kernels derived by white-noise methods to predict the responses of fly photoreceptors to moving points of light. Because pursuit stimuli and responses differ considerably from white noise in waveform and amplitude (Fig. 2), we compared recorded pursuit responses with the predictions of white-noise analysis.

First- and second-order Wiener kernels, constructed from responses to Gaussian white noise (see Materials and methods), were used to predict the average responses of individual photoreceptors, both to a further white-noise

stimulus and to representative pursuit stimuli. We confirmed that fly photoreceptors behave remarkably linearly in response to white noise (French, 1980; Juusola et al., 1994). The mean squared error between the linear (first order) prediction and the average response to white noise was typically 5%. This figure was only marginally improved when the second-order kernel was introduced (not shown).

When predicting responses to pursuit stimuli (Fig. 8), the first-order (linear) kernel works well at the lowest response amplitudes (distant targets), as demonstrated in Fig. 8A where real and predicted responses overlap. However, with increased stimulus contrast and photoreceptor response amplitude (Fig. 8B), the first-order prediction (dotted line) captures only 75% of the peak-to-peak response amplitude of the real response (solid line), and the second-order kernel is required to produce a reasonable approximation (broken line). With longer duration pursuit stimuli even the second-order kernel becomes inadequate. The recorded response to a 15° target moving at 300 deg. s^{-1} is almost 30% larger than predicted from the second-order model (Fig. 8C, c.f. solid and broken lines). The same width target moving at 10 deg. s^{-1} elicits a response that is not only 70% larger than predicted but is also biphasic (Fig. 8D). Similar differences are observed in the responses to a 3° target moving at 1000 deg. s^{-1} (Fig. 8E) or 10 deg. s^{-1} (Fig. 8F). While the second-order kernel predicts the same amplitude response in both cases, the recorded response is substantially larger for the longer stimulus.

Thus, although the photoreceptor behaves remarkably linearly to white-noise stimuli, white-noise analysis does not predict the responses to many of the moving targets that male flies track during pursuit.

Discussion

The pursuit of one housefly by another is a well-defined behaviour, apparently directed by a few simple target cues. Taking published measurements of target angular width and angular speed, we have constructed the changes in light intensity experienced by single photoreceptors as targets move across their fields of view. The larger facet lenses, higher sampling density and faster electrical responses of male-specific 'lovespot' photoreceptors must improve the resolution of small fast-moving targets (Hornstein et al., 2000; Land, 1997). By recording the responses of male and female photoreceptors to our stimuli we have determined the quality of the retinal images generated in both sexes during pursuit and quantified the contribution of male photoreceptors to the male's superior pursuit performance.

Previous studies have examined the resolution of the insect eye for moving objects using point stimuli (Juusola and French, 1997; Srinivasan and Bernard, 1975). In both cases, the responses of photoreceptors to these stimuli are made from impulse responses obtained using conventional analytical stimuli (flashes or Gaussian white noise). Our study differs from this work because we have recorded photoreceptor responses directly to pursuit stimuli. Our direct approach
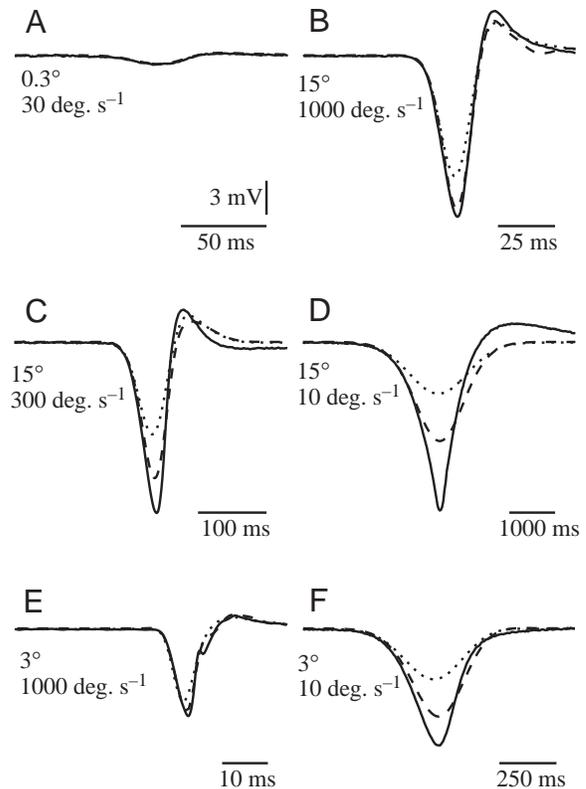

Fig. 8. White-noise analysis does not predict pursuit responses. (A–F) Responses (solid line) of a male photoreceptor to selected pursuit stimuli are compared with those predicted from first-order (dotted line) and second-order (broken line) kernels from white-noise analysis. The voltage scale for all plots is the same (scale bar in A). The kernel predictions often underestimate the true response and comparison of (E) and (F) suggests that stimulus duration, not just the final predicted potential, is responsible for these differences.

demonstrates specializations that are not predicted from responses to conventional analytical stimuli. We find the male photoreceptor has a distinct optimum target speed (Figs 4, 5), a feature more reminiscent of previous predictions of interneurone responses (large monopolar cells) than of photoreceptor responses (Juusola and French, 1997). A non-linear dependence of response on contrast boosts responses to near targets, particularly in the male (Fig. 6). The spatial resolution of moving targets is higher than expected, particularly at lower speeds where the blur factor is less than 1 in both sexes (Fig. 5). This reduction contradicts the prediction from impulse responses (Juusola and French, 1997) that response width asymptotes to the optical width of the target at low angular speeds.

We suggest that Gaussian white-noise (GWN) analysis fails to predict pursuit responses because pursuit stimuli cover a larger range of contrasts than GWN can adequately test. GWN is concentrated near its mean. Consequently, GWN predictions of responses to high-contrast stimuli are largely based upon extrapolation, a notoriously unreliable procedure. This problem is especially acute for longer stimuli (Fig. 8) because

these have particularly powerful low-frequency components. Such stimuli are not prominent features of GWN, which by definition spreads power equally across all frequencies.

We have also, unlike previous work, considered target distance and angular width. An assumption that targets can be modelled as point sources is invalid for much of the chase. Because near objects are large, they can be moving at very high angular speeds before significant blurring occurs or response amplitude falls. Thus, like Juusola and French (1997), we find that the response to small (point) or distant targets starts to deteriorate at 200 deg. s^{-1}, but for near targets the male photoreceptor's optimum response is at approximately 1000 deg. s^{-1} (Fig. 4). Generally, when we convert angular speeds (ω) to absolute flight speeds (u) (Fig. 5), male responses easily follow a female at natural speeds (60 cm s^{-1}). This observation has implications for understanding the neural mechanisms of tracking: photoreceptors rarely compromise target tracking during pursuit.

Target detection

In an ideal observer task we found that the male photoreceptor generates a detectable response to a cruising fly at a distance of at least 76 cm (Fig. 3). The female performs similarly at slightly less than half this distance (33 cm). The difference primarily reflects superior male optics. The distance at which the optical image exceeds a given contrast is inversely proportional to photoreceptor acceptance angle (Equations 7,11; see Materials and methods) and the lovespot acceptance angle is half the female value. Optics therefore play a crucial role in determining target detectability.

What is surprising, however, is how far behavioural measurements fall short of these photoreceptor limits. The male housefly gives chase when the leading fly is only 20 cm directly ahead, although there is evidence for orientation at 25 cm (Wagner, 1986b). What could be the reasons for this discrepancy? One is simply that behavioural measurements have been taken indoors where, with lower light levels, the signal-to-noise ratio (d') is much less than we were able to obtain with an LED. It is also likely that the assumptions of the 'ideal observer' model are inappropriate. In the model we assume that the stimulus-present and stimulus-absent trials are equally probable, that identification of either condition carries equal pay-off, and that the fly knows both what the stimulus will be (for optimal filtering purposes) and when in a trial that stimulus can occur. The natural situation may encourage more cautious decision-making than these assumptions generally allow. For example, pay-offs are not equal. A 'positive' choice always incurs the energetic cost of chasing, but may not result in a successful mating if the target is misidentified or other males have intercepted the target first (see Collett and Land, 1978; Thornhill, 1980). These factors might raise the decision threshold despite the reproductive forfeit of a false negative decision.

Still another reason for discrepancy might be that the fly is accustomed to operating in a more cluttered environment where image distractors are the dominant noise source. Although males try to chase targets against the sky, initial detection may be against a complex background, inevitably making the detection task more difficult. We have argued that male photoreceptor responses are adjusted to respond preferentially to moving targets. How they perform in 'image noise' is a matter of some interest. We suggest that the non-linear contrast gain of male photoreceptors may be an adaptation for amplifying the higher contrast targets against lower contrast clutter.

Pursuit responses

Once detected, a target fly is vigorously chased at distances associated with angular widths of 3–30°. For 80% of the chase the male keeps the target in the lovespot with an angular speed in the range 100–1000 deg. s^{-1} (Wagner, 1986b). The lovespot photoreceptor is maximally responsive over this range of target angles and speeds (Fig. 4A) and its image of a target is always sharper than its female counterpart (Fig. 4C,D). Naturally, fast-moving episodes are very brief and, therefore, they may be of limited importance for flight control, but there is no doubt that during such episodes, lovespot photoreceptors register target position.

We have identified and assessed the factors that improve the responses of lovespot photoreceptors to 'chased' targets: optics, photoreceptor gain and photoreceptor response dynamics. Lovespot lenses, with their narrow acceptance angles, deliver shorter, higher contrast stimuli than female optics. However, at chasing distances, where targets fill the acceptance angles of both sexes, superior male optics provide much less of an advantage than they do in the detection regime. Consequently, it is mostly the lovespot photoreceptor that elevates performance during chasing.

At most speeds and for all contrasts, the gain of a lovespot photoreceptor is 3–4 times the female value. Consequently the male responses to pursuit stimuli are surprisingly large, reaching 25 mV in some animals. The way in which these large male responses to moving targets are achieved is not clear, but we can suggest some possibilities. First and foremost, the faster response of the lovespot photoreceptor increases bandwidth (Hornstein et al., 2000) and hence the amplitude of responses to the rapidly changing pursuit stimuli. This effect may then be amplified by self-shunting. As the light-gated channels close due to the presence of a dark target, the resistance of the membrane increases and the membrane voltage becomes more sensitive to further channel closure. Such a mechanism could explain why contrast gain increases with stimulus contrast.

This type of non-linear contrast gain function is thought to contribute to the ability of the human visual system to deblur moving images (Hammett et al., 1998). Neural deblurring is a prominent feature of the male photoreceptor's response where the pronounced transient, symptomatic of high-pass filtering in phototransduction (Hornstein et al., 2000), reduces the spread of the response to a moving target in the direction of motion (Fig. 6). Interestingly, high-pass filtering is also thought to contribute to deblurring in the human visual system (Pääkkönen and Morgan, 2001).

Amplification depends as much on the duration of the

stimulus (over two orders of magnitude) as either its contrast or the final voltage predicted from white-noise kernels (compare Fig. 8E with F). This observation suggests that the male response could be boosted by time-dependent mechanisms, such as voltage-sensitive ion channels. In drone bee retina tetrodotoxin-sensitive Na^+ channels amplify the responses to the small brief decrements in intensity produced by over-flying queen bees (Coles and Schneider Picard, 1989) and operate best in the behavioural response range (Vallett and Coles, 1993). Voltage-gated Ca^{2+} channels at the photoreceptor's synaptic terminal could play a similar role in fly (Weckström et al., 1992).

Adapting retinal photoreceptors and neurones to behavioural stimuli

It is well established that photoreceptor arrays can be tuned to specific behavioural tasks (Lythgoe, 1979; Wehner, 1987). For several animals, these tasks include the detection of mates or prey. Photoreceptor spectral sensitivity and spatial and temporal properties may each be adapted for this purpose (Attwell et al., 1984; Cronin et al., 2000; Vallet and Coles, 1993; Zeil et al., 1986). Using a behaviourally relevant set of stimuli, we have shown that photoreceptor responses in the male housefly *Musca domestica*, but not the female, are well suited to the target speeds normally experienced during the pursuit of conspecifics, a behaviour exhibited by males prior to mating. This finding is perhaps a rudimentary example of the principle of matched filtering (Wehner, 1987). Might other early visual neurones also show special pursuit responses?

A natural place to explore this issue further is in the fly's postsynaptic large monopolar cells (LMCs). Although LMCs transmit information as graded potentials, the LMCs, L1 and L3, will elicit 'off'-spikes when photoreceptors hyperpolarise deeply and quickly in sequence (Hardie and Weckström, 1990; Uusitalo et al., 1995). Thus, the single off-spike could mark fast, high-contrast targets. In this regard, it is interesting that one of the spiking LMCs, L3, is larger in the lovespot than anywhere else in the male or female eye (Braitenberg, 1972). We suggest that L3 may prove to be a filter for moving targets, activated by large photoreceptor responses.

List of Symbols

General

θ	2-D angular position (deg., deg.)
t	time (s)
f	frequency (Hz)

Stimulus construction

$\theta_x(t)$	angular position of target (deg., deg.)
ϕ	eccentricity of target from photoreceptor's optical axis (deg.)
$X(\theta,t)$	relative intensity of target (no units)
$L(\theta)$	point spread function (PSF) of optics (deg.$^{-2}$)
$\Delta\rho$	angular width at half maximum height of PSF (deg.)
$I(\theta,t)$	optical image of target (no units)
$C(t)$	contrast stimulus delivered to photoreceptor (no units)

Target and stimulus parameters

b	true width of target (cm)
s	distance of target from eye (cm)
u	target flight speed (cm s^{-1})
$\Delta\rho_x$	angular width of target at half peak contrast, seen at eye (deg.)
ω	angular speed of target, seen at eye (deg. s^{-1})
ΔC	stimulus contrast amplitude (no units)
$\Delta\rho_c$	angular half-width of target after optical blurring (deg.)
τ_c	stimulus duration at half peak contrast (s)
ΔV	photoreceptor response amplitude (mV)
$\Delta\rho_v$	angular width of neural image at half peak response (deg.)
τ_v	photoreceptor response duration at half peak response (s)

Target detection

$\bar{v}(t)$	mean photoreceptor response to target (mV)
$\bar{V}(f)$	Fourier transform of $\bar{v}(t)$ (mV Hz^{-1})
$N(f)$	power spectrum of photoreceptor noise (mV^2 Hz^{-1})
$h(t)$	impulse response of noise suppression filter (mV^{-1} s^{-1})
$H(f)$	Fourier transform of h(t) (mV^{-1})
$\mathbf{A}$	filtered response amplitude (no units)
$E[\mathbf{A}]$	expected filtered response amplitude (no units)
σ	standard deviation of filtered photoreceptor noise (no units)
d'	signal-to-noise ratio of target (no units)

References

Atick, J. J. and Redlich, A. N. (1992). What does the retina know about natural scenes? *Neural Comp.* **4**, 196-210.

Attwell, D., Wilson, M. and Wu, S. M. (1984). A quantitative analysis of interactions between photoreceptors in the salamander *(Ambystoma)* retina. *J. Physiol.* **352**, 703-737.

Braitenberg, V. (1972). Periodic structures and structural gradients in the visual ganglia of the fly. In *Information Processing in the Visual Systems of Arthropods* (ed. R. Wehner), pp. 3-15. Berlin: Springer.

Burton, B. G., Tatler, B. W. and Laughlin, S. B. (2001). Variations in photoreceptor response dynamics across the fly retina. *J. Neurophysiol.* **86**, 950-960.

Camhi, J. M. (1984). *Neuroethology: Nerve Cells and the Natural Behaviour of Animals*. Sunderland, Sinauer.

Coles, J. A. and Schneider-Picard, G. (1989). Amplification of small signals by voltage-gated sodium channels in drone photoreceptors. *J. Comp. Physiol. A* **165**, 109-118.

Collett, T. S. and Land, M. F. (1978). How hoverflies compute interception courses. *J. Comp. Physiol.* **125**, 191-204.

Cronin, T. W., Järvilehto, M., Weckström, M. and Lall, A. B. (2000). Tuning of photoreceptor spectral sensitivities in fireflies. *J. Comp. Physiol. A* **186**, 1-12.

French, A. S. (1980). The linear dynamic properties of phototransduction. *J. Physiol.* **308**, 385-401.

Green, D. M. and Swets, J. A. (1966). *Signal Detection Theory and Psychophysics*. New York: Wiley.

Hammett, S. T., Georgeson, M. A. and Gorea, A. (1998). Motion blur and

motion sharpening: temporal smear and local contrast non-linearity. *Vision Res.* **38**, 2099-2108.

Hardie, R. C. (1979). Electrophysiological analysis of the fly retina. 1. Comparative properties of R1-6 and R7 and R8. *J. Comp. Physiol.* **129**, 19-33.

Hardie, R. C. (1985). Functional organisation of the fly retina. In *Progress in Sensory Physiology*, vol. 5 (ed. D. Ottoson), pp. 1-79. Berlin: Springer-Verlag.

Hardie, R. C. and Weckström, M. (1990). Three classes of potassium channels in large monopolar cells of the blowfly, *Calliphora vicina*. *J. Comp. Physiol. A* **167**, 723-736.

van Hateren, J. H. (1992). Theoretical predictions of spatiotemporal receptive fields of fly LMCs and experimental validation. *J. Comp. Physiol. A* **171**, 157-170.

van Hateren, J. H. (1997). Processing of natural time series of intensities by the visual system of the blowfly. *Vision Res.* **37**, 3407-3416.

van Hateren, J. H. and Snippe, H. P. (2001). Information theoretical evaluation of parametric models of gain control in blowfly photoreceptor cells. *Vision Res.* **41**, 1851-1865.

Hornstein, E. P., O'Carroll, D. C., Anderson, J. C. and Laughlin, S. B. (2000). Sexual dimorphism matches photoreceptor performance to behavioural requirements. *Proc. R. Soc. Lond. B* **267**, 2111-2117.

Juusola, M. and French, A. S. (1997). Visual acuity for moving objects in first and second order neurons of the fly compound eye. *J. Neurophysiol.* **77**, 1487-1495.

Juusola, M., Kouvalainen, E., Järvilehto, M. and Weckström, M. (1994). Contrast gain, signal-to-noise ratio and linearity in light-adapted blowfly photoreceptors. *J. Gen. Physiol.* **104**, 593-621.

Land, M. F. (1997). Visual acuity in insects. *Ann. Rev. Entomol.* **42**, 147-177.

Land, M. F. and Collett, T. S. (1974). Chasing behaviour of houseflies (*Fannia canicularis*). *J. Comp. Physiol.* **89**, 331-357.

Land, M. F. and Eckert, H. (1985). Maps of the acute zones of fly eyes. *J. Comp. Physiol.* **156**, 525-538.

Laughlin, S. B. (1981). A simple coding procedure enhances a neurone's information capacity. *Z. Naturforsch.* **36**, 910-912.

Laughlin, S. B., Howard, J. and Blakeslee, B. (1987). Synaptic limitations to contrast coding in the retina of the blowfly *Calliphora*. *Proc. R. Soc. Lond. B* **231**, 437-467.

Lythgoe, J. N. (1979). *The Ecology of Vision*. Oxford: Clarendon Press.

Marmarelis, P. Z. and Marmarelis, V. Z. (1978). *Analysis of Physiological Systems. The White-noise Approach*. New York: Plenum Press.

Pääkkönen, A. K. and Morgan, M. J. (2001). Linear mechanisms can produce motion sharpening. *Vision Res.* **41**, 2771-2777.

Papoulis, A. (1991). *Probability, Random Variables and Stochastic Processes*, 3rd edn. New York: McGraw-Hill.

Reinagel, P. (2001). How do visual neurons respond in the real world? *Curr. Opin. Neurobiol.* **11**, 437-442.

Rinberg, D. and Davidowitz, H. (2000). What do cockroaches 'know' about fluid dynamics? *Nature* **405**, 756.

Schilstra, C. and van Hateren, J. H. (1999). Blowfly flight and optic flow. I. Thorax kinematics and flight dynamics. *J. Exp. Biol.* **202**, 1481-1490.

Simoncelli, E. P. and Olshausen, B. A. (2001). Natural image statistics and neural representation. *Ann. Rev. Neurosci.* **24**, 1193-1215.

Smakman, J. G. J. and Stavenga, D. G. (1987). Angular sensitivity of blowfly photoreceptors: broadening by artificial electrical coupling. *J. Comp. Physiol. A* **160**, 501-507.

Snyder, A. W. (1979). Physics of vision in compound eyes. In *Handbook of Sensory Physiology*, vol. VII/6A (ed. H. Autrum), pp. 225-313. Berlin: Springer-Verlag.

Srinivasan, M. V. and Bernard, G. D. (1975). The effect of motion on visual acuity of the compound eye: a theoretical analysis. *Vision Res.* **15**, 515-525.

Srinivasan, M. V. and Bernard, G. D. (1977). The pursuit response of the housefly and its interaction with the optomotor response. *J. Comp. Physiol.* **115**, 101-117.

Thornhill, R. (1980). Sexual selection within mating swarms of the lovefly, *Plecia nearctica* (Diptera: Bibionidae). *Anim. Behav.* **28**, 405-412.

Uusitalo, R. O., Juusola, M. and Weckström, M. (1995). Graded responses and spiking properties of identified first-order visual interneurons of the fly compound eye. *J. Neurophysiol.* **73**, 1782-1792.

Vallet, A. M. and Coles, J. A. (1993). The perception of small objects by the drone honeybee. *J. Comp. Physiol A* **172**, 183-188.

Wagner, H. (1986a). Flight performance and visual control of flight of the free-flying housefly, *Musca domestica*. I. Organization of the flight motor *Phil. Trans. R. Soc. Lond. B* **312**, 527-551.

Wagner, H. (1986b). Flight performance and visual control of the free-flying housefly, *Musca domestica*. II. Pursuit of targets. *Phil. Trans. R. Soc. Lond. B* **312**, 553-579.

Weckström, M., Juusola, M. and Laughlin, S. B. (1992). Presynaptic enhancement of signal transients in photoreceptor terminals in the compound eye. *Proc. R. Soc. Lond. B* **250**, 83-89.

Wehner, R. (1987). 'Matched filters' – neural models of the external world. *J. Comp. Physiol A* **161**, 511-531.

Wehrhahn, C. (1979). Sex-specific differences in the chasing behaviour of houseflies *Musca*. *Biol. Cybern.* **32**, 239-241.

Wehrhahn, C. and Hausen, K. (1980). How are tracking and fixation accomplished in the nervous system of the fly? *Biol. Cybern.* **38**, 179-186.

Wehrhahn, C., Poggio, T. and Bulthoff, H. (1982). Tracking and chasing in houseflies (*Musca*). *Biol. Cybern.* **45**, 123-130.

Zeil, J., Nalbach, G. and Nalbach, H. O. (1986). Eyes, eye stalks and the visual world of semi-terrestrial crabs. *J. Comp. Physiol. A* **159**, 801-811.